European Conference on Optical Communication (ECOC) 2022 ©
Optica Publishing Group 2022

Integrated Optical Phased Array For Circularly Polarized Orbital Angular Momemtum Multiplexing

Yuxuan Chen, Simon Levasseur, Leslie A.Rusch, Wei Shi*

(1) Department of Electrical and Computer Engineering, Centre for Optics, Photonics and Lasers, Université Laval, Québec, QC, Canada, wei.shi@gel.ulaval.ca

Abstract *We design and demonstrate an on-chip tunable optical phased array that generates multiplexed circularly polarized Orbital Angular Momemtum modes with record performance (24 simultaneous modes, -16.4dB worst-case crosstalk).*

Introduction

Spatial division multiplexing (SDM) is a crucial technology for scaling data transmission[1]. Ring core fibers that support orbital angular momemtum (OAM) modes are a promising SDM solution for short-reach fiber transmission links with the ability of providing tens of parallel data channels with less complex Multiple-input and multiple-output digital signal processing[2]. Spatial light modulators or vortex plates are often used in free-space setups to generate high-purity OAM modes, followed by wave-plates for exciting circularly polarized modes in OAM fiber. These setups are usually bulky.

Integrated devices based on ring-resonators[3], waveguide surface holographic gratings[4] and star couplers[5] were demonstrated for compact OAM generator and multiplexers (MUX) in photonic integrated circuits. However, these devices require off-chip polarization management to achieve a circularly polarized mode, while fiber propagation (unlike free space) OAM requires circular polarization. Our previous work demonstrated a broadband OAM multiplexer using an optical phased array (OPA) with 2-dimensional (2D) antennas for on-chip circularly polarized OAM beam generation[6]. However, this device suffers from non-uniform intensity distribution in presence of fabrication errors, causing a relative high-level of crosstalk.

In this work, we demonstrate, for the first time, an OPA-based OAM multiplexer with an intensity tuning circuit that substantially improves the OAM quality by enabling a uniform power distribution across the antennas. Moreover, compared to our previous work[6], the number of antennas is increased to 27 for a better phase resolution and for higher-order OAM mode generation. The device supports the highest number of OAM modes (24, i.e., 12 per circular polarization) and the lowest worst-case crosstalk (-16.4dB) ever reported on a silicon chip.

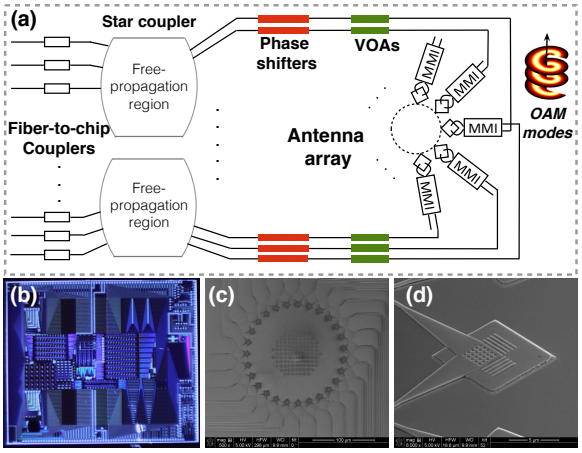

Fig. 1: (a) Schematic of the proposed OAM generator and multiplexer, (b) Photograph of the fabricated device, (c) SEM image of the antenna array, and (d) SEM image of one 2D antenna.

Design and fabrication

The schematic of the proposed OAM generator and multiplexer is presented in Fig. 1a. A fiber array inputs data signals to the fiber-to-chip couplers on the left side of the OAM MUX circuit. The couplers guide the light to distinct positions on the left side of the star coupler free-propagation region. This creates for each input a distinct phase distribution at the star coupler output. The geometry of the star coupler is judiciously designed so that each phase distribution creates a unique skewed phase, one for each targeted OAM state. Each path after the star coupler has a thermally controlled phase shifter and a variable optical attenuator (VOA) in a p-i-n silicon waveguides. These tunable components allow us to compensate for phase errors and intensity imperfections.

An array of 27 2D antennas is placed along a 165 μm circumference, and are designed for C band. Each antenna has five grating periods of 570nm (in both direction), a hole size of 390nm diameter, and four periods of grating re-

flector (505nm period, 0.5 fill factor). The device is design for C-band using the model presented[7] and parameters compatible with a typical 193-nm optical lithography foundry process.

The chip was fabricated at Advanced Micro Foundry Inc. A top view of the fabricated chip is shown in Fig. 1b. In the SEM image (Fig. 1c), we see the array of 2D antennas evenly-spaced with central axis pointing toward the center of the circumference. Each 2D antenna is connected to a 2×2 MMI through 5μm bents. The 2×2 MMI creates ±90 degree phase difference between two linear polarization inputs (quasi-TE modes in our design), enabling on-chip circularly polarized beam generation. A magnified view at 50° tilt of one 2D antenna is shown in Fig. 1d, where the square around the grating region is the shallow-etched silicon layer at 150μm thickness.

Chip characterization

We perform a two-step calibration to adjust the intensity and phase of light in all paths before they reach the antenna array. We use an optical cage system for a stable experimental environment during calibration and characterization. The single channel performance is characterized by using the device as a de-multiplexer (DeMUX) for the fundamental mode and measuring the worst-case crosstalk among all supported modes. The device is tested as a MUX by observing interference patterns that validate OAM generation.

In the first calibration step (intensity tuning) we generate the OAM0 mode. The device splits light within the free-propagation region, where light diverges and inevitably ends up with a Gaussian-like intensity distribution in the lateral direction. If left untouched, this distribution is mapped onto the antenna array and forms a crescent shaped near-field intensity pattern, rather than a high purity OAM mode with circular symmetry. Our intensity tuning circuit corrects the non-uniformity by applying attenuation to high power paths. To identify paths and quantify attenuation, we generate an OAM0 mode with our device, and monitor the near field on the camera. A 4-f system, lens L1 (10mm focus) and L2 (50mm focus), provides five times magnification and antenna spots are clearly separated in the camera (Fig. 2, path 1, dashed blue line). The intensity distribution before tuning is shown in Fig. 4a, the spots top-right are visibly dimmer than the spots bottom-left. We apply tuning signals onto the VOAs based on the camera data. A more uniform intensity distribution is visible in Fig. 4b after tuning.

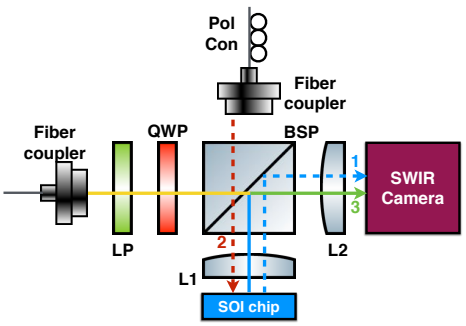

Fig. 2: Setup for intensity tuning (blue dashed path 1), phase error correction (red dashed path 2) and interferograms (solid path 3); LP: linear polarizer, QWP: quarter waveplate, BSP: non-polarizing beamsplitter, L1: 10mm focus lens, L2: 50mm focus lens, Pol con: polarization controller

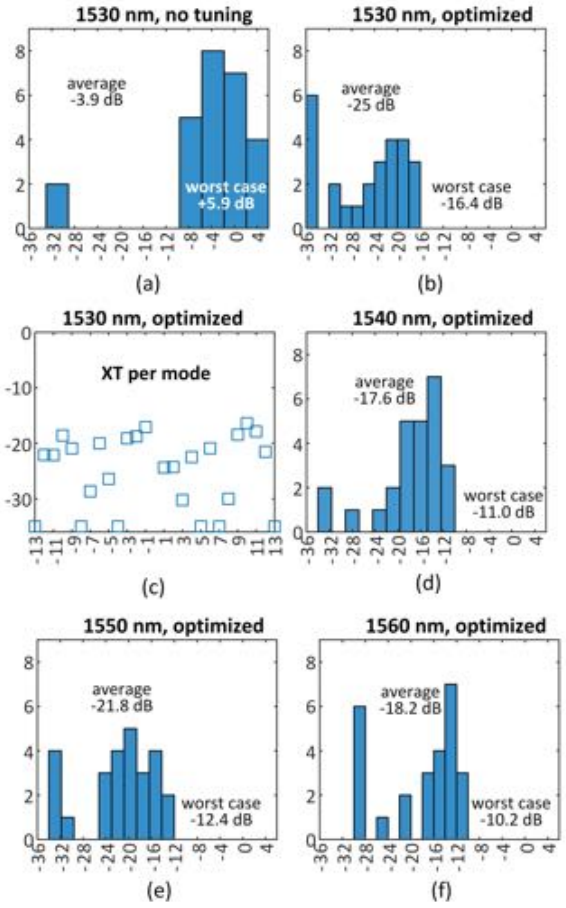

Fig. 3: Crosstalk histograms (a) before tuning, and (b), (d), (e) and (f) after tuning, crosstalk in x axis, number of modes in y axis; and (c) XT per mode after tuning.

In the second calibration step (phase tuning) we use the device as DeMUX. Following path 2 (dashed red line) in Fig. 2, a circularly polarized OAM0 (Gaussian) is projected onto the antenna array. The Gaussian is DeMUXed by our device into 27 OAM modes, each converted to fundamental mode and output to a fiber. All power is routed to the OAM0 output fiber if fabrication is perfect. The power to other modes creates crosstalk. We monitor power at each of the 27

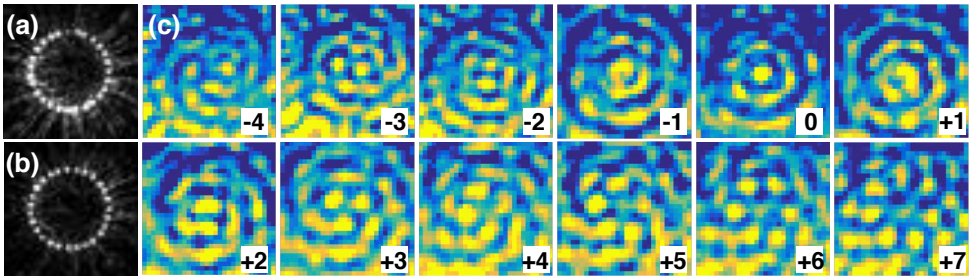

Fig. 4: Near-field intensity distribution of generated OAM0 (a) without intensity tuning, and (b) with intensity tuning; and (c) Interference pattern for OAM-4 to OAM+7, number of spirals equal to their topological charge

output fibers (left of the fiber-to-chip coupler in Fig. 1a). We continuously monitor power while applying phase tuning until optimum worst-case crosstalk is reached. We use a gradient descent algorithm for finding the optimum tuning. The routing waveguides are 65μm apart, so that the thermal crosstalk is negligible. The metal heaters, 750nm above the routing waveguides, increase the local temperature when tuned, changing the effective index and phase. These challenges are discussused in the next section.

In Fig. 3a we show the histogram of crosstalk on OAM0 before phase tuning at 1530nm. Among 26 unwanted modes, 19 modes have crosstalk higher than -4dB. Our phase tuning algorithm dynamically identifies the worst-crosstalk mode and suppresses the power in that mode, then continues iteration. The worst case crosstalk is improved to -16.4dB (Fig. 3b), with an average crosstalk of -25dB. In Fig. 3c, we see no particular pattern in XT across mode orders. We achieve around -11dB worst case crosstalk at 1540nm, 1550nm and 1560nm with the same tuning procedure. At all wavelengths we use the same set of voltages for tuning; the mesh of phases happens to work best at 1530nm. We anticipate the same or potentially better performance over C band when optimizing the mesh.

We evaluate the generation of modes other than the fundamental by producing an interferogram by removing L2 from the right side of the setup in Fig. 2. The generated beam from our device (solid blue line) is collimated by L1. A reference Gaussian is circularly polarized after passing through a polarizer and a quarter waveplate (solid yellow line). The generated beam and the reference Gaussian propagate colinearly along path 3 (solid green line) and the interference is captured on the camera. Fig. 4c shows the interference patterns for OAM -4 to +7. The origins of the spirals appear as bright spots in the center of the image, the arms follow, in number equal to the OAM topological charge. Spirals for OAM -5 to -7 are not shown as their spiral arms are difficult to distinguish; we suspect the fiber-to-chip couplers involved in their generation are more lossy.

Experimental challenges

The limiting factor of the tuning process is the setup stability against thermal effects. For the calibration of one circular polarization, the 27 VOAs consume about 2W of power; sweeping the 27 phase shifters require another 1W. We prepared a robust heat sink for our packaged assembly. We integrated a temperature sensor to monitor the chip temperature while tuning. During the phase calibration, as we sweep the voltage on the phase shifter, the temperature of the tuned waveguide can change up to 40°C and is constantly varying.

We use a Peltier cooler to drain heat toward the heat sink when the temperature rises, and stabilize the chip around room temperature. Nevertheless, a local temperature change, not necessarily large enough to cause detectable chip temperature rise, can cause phase shifts that lead to misalignment. A packaging plan with improved heat dissipation, or with OAM fiber coupling at the antenna array, can reduce system uncertainty and accommodate better calibration accuracy.

Conclusion

We design and characterize an optical phased array on a SOI platform that directly generates and multiplexes circularly polarized OAM modes. The device benefits from an intensity tuning circuit and achieves record low worst-case crosstalk (-16.4dB). We confirm generation of 24 OAM modes via spiral interference patterns, significantly extending the capacity of previous WDM-compatible silicon-based OAM multiplexers. The device provides a scalable, integrated solution for OAM generation and multiplexing in ultra-high capacity SDM systems.

Acknowledgements

We thank Nathalie Bacon for suggestions in setup building and arrangement.

References

[1] P. J. Winzer, D. T. Neilson, and A. R. Chraplyvy, "Fiber-optic transmission and networking: The previous 20 and the next 20 years", *Optics express*, vol. 26, no. 18, pp. 24 190–24 239, 2018.

[2] M. Banawan, S. K. Mishra, S. LaRochelle, and L. A. Rusch, "Modal loss characterisation of thick ring core fiber using perfect vortex beams", in *Optical Fiber Communication Conference*, Optica Publishing Group, 2022, W3E–5.

[3] S. Li, Z. Nong, X. Wu, *et al.*, "Orbital angular momentum vector modes (de) multiplexer based on multimode micro-ring", *Optics express*, vol. 26, no. 23, pp. 29 895–29 905, 2018.

[4] N. Zhou, S. Zheng, X. Cao, *et al.*, "Ultra-compact broadband polarization diversity orbital angular momentum generator with 3.6$\times$ 3.6 μm2 footprint", *Science advances*, vol. 5, no. 5, eaau9593, 2019.

[5] B. Guan, C. Qin, R. P. Scott, *et al.*, "Polarization diversified integrated circuits for orbital angular momentum multiplexing", in *2015 IEEE Photonics Conference (IPC)*, IEEE, 2015, pp. 649–652.

[6] Y. Chen, Z. Lin, S. Bélanger-de Villers, L. A. Rusch, and W. Shi, "Wdm-compatible polarization-diverse oam generator and multiplexer in silicon photonics", *IEEE Journal of Selected Topics in Quantum Electronics*, vol. 26, no. 2, pp. 1–7, 2019.

[7] Y. Chen, L. A. Rusch, and W. Shi, "Integrated circularly polarized oam generator and multiplexer for fiber transmission", *IEEE Journal of Quantum Electronics*, vol. 54, no. 2, pp. 1–9, 2017.